A&A 539, A136 (2012)
DOI: 10.1051/0004-6361/201118134

Astronomy & Astrophysics

Stellar metallicity of star-forming galaxies at $z \sim 3$⋆

V. Sommariva[1], F. Mannucci[1,2], G. Cresci[1], R. Maiolino[3], A. Marconi[4], T. Nagao[5], A. Baroni[4], and A. Grazian[3]

[1] INAF – Osservatorio Astrofisico di Arcetri, Firenze, Italy
e-mail: veronica@arcetri.astro.it
[2] Harvard-Smithsonian Center for Astrophysics, 60 Garden street, Cambridge, MA 02138, USA
[3] INAF – Osservatorio Astronomico di Roma, Monte Porzio Catone, Italy
[4] Dipartimento di Astronomia, Università di Firenze, Firenze, Italy
[5] Kyoto University, Japan

Received 22 September 2011 / Accepted 9 December 2011

ABSTRACT

The stellar metallicity is a direct measure of the amount of metals present in a galaxy, since a large part of the metals lie in its stars. In this paper, we investigate new stellar metallicity indicators suitable for high-z galaxies by studying the stellar photospheric absorption lines in the rest-frame ultraviolet, hence sampling predominantly young hot stars. We defined these new indicators based on the equivalent widths (EW) of selected features using theoretical spectra created with the evolutionary population synthesis code Starburst99. We used them to compute the stellar metallicity for a sample of ultraviolet-selected galaxies at $z > 3$ from the AMAZE (Assessing the Mass-Abundance redshift Evolution) survey using very deep (37 h per object) VLT/FORS spectra. Moreover, we applied these new metallicity indicators to eight additional high redshift galaxies studied in literature. We then compared stellar and gas-phase metallicities measured from the emission lines for all these galaxies, finding that within the errors the two estimates are in good agreement, with possible tendency for stellar metallicities to be lower than the gas phase ones. For the first time, we study the stellar mass-stellar metallicity relation at $z > 3$. We find that the metallicity of young, hot stars in galaxies at $z \sim 3$ have similar values of the aged stars in local SDSS galaxies, in contrast to findings for the gas phase metallicity.

Key words. galaxies: evolution – galaxies: high-redshift

1. Introduction

Metallicity is one of the most important properties of galaxies, and its study is able to shed light on the details of galaxy evolution. It is an integrated property, related to the whole past history of the galaxies. In particular, metallicity is sensitive to the entire star formation history, hence to the evolutionary stage of the galaxy. Moreover, it is affected by the presence of infalls and outflows, i.e. by feedback processes and the interplay between the forming galaxy and the intergalactic medium (see e.g. Erb 2008; Mannucci et al. 2009; Cresci et al. 2010). As a consequence, it has become an important test of galaxy evolution (e.g. Nagamine et al. 2001; Spitoni et al. 2010; Davé et al. 2011).

Local galaxies follow a clear correlation between mass and metallicity (MZR), for which the galaxies with higher stellar masses have higher metallicities, and this correlation appears to hold for both gas-phase metallicity (e.g. Tremonti et al. 2004) and stellar metallicity (Gallazzi et al. 2005; Panter et al. 2008).

At high redshift, the gas-phase metallicity of the ISM of star-forming galaxies has been measured using primarily oxygen abundances. The most common techniques to determine the gas phase metallicity are based on either theoretical calibrations (see Kewley & Dopita 2002; Kewley & Ellison 2008) or empirical metallicity calibrations, the so-called "strong line diagnostics", which are based on the ratios of collisionally excited forbidden lines to hydrogen recombination lines. Previous studies have shown that the mass-gas phase metallicity relation provides evidence of strong redshift evolution. Among others, Savaglio et al. (2005) and Zahid et al. (2011) studied star forming galaxies at redshift $z \sim 0.7$ and demonstrated that, at a given mass, these galaxies have lower metallicities than the SDSS sample at $z \sim 0.1$. Erb et al. (2006) reported a more significant decrease in metallicity for galaxies at $z \sim 2.2$. Two projects were specifically designed to extend the investigation of MZR at $z > 3$: the LSD (Lyman-break Stellar population and Dynamic) and AMAZE (Assessing the Mass-Abundance redshift Evolution) surveys. With these projects, Maiolino et al. (2008) and Mannucci et al. (2009) showed for the first time the evolution of the mass-metallicity relation at $z > 3$. However, the redshift evolution of the gas phase metallicity in galaxies was questioned by Mannucci et al. (2010). They discovered that metallicity depends not only on mass, but also on the star formation rate (SFR): for a given stellar mass, galaxies with higher SFRs have systematically lower metallicities. This is the so-called "fundamental metallicity relation (FMR)", i.e., a tight relation between stellar mass, gas-phase metallicity, and star formation rate (SFR). Local SDSS galaxies have very small residuals about this relation, of the order of 0.05 dex. Yates et al. (2011) found a similar relation, with some differences owing to the metallicity calibration adopted. According to Mannucci et al. (2010), the FMR does not appear to evolve with redshift up to $z \sim 2.5$, with the high redshift galaxies following the same FMR as local SDSS galaxies. This suggests that the observed evolution of the mass-metallicity relation is due to selection effects and the increasing the average SFR with redshift. The measured metallicity in several additional samples of high-z galaxies indeed agree with the predictions of the FMR given the

⋆ Based on ESO observations, proposals 082.A-0398 and 084.A-0367.

mass and SFR of the galaxies: galaxies with lower SFRs than the general population at their redshifts also have higher metallcities (e.g., Richard et al. 2011; Nakajina et al. 2012), and galaxies with higher SFRs also have lower metallicities (e.g., Erb et al. 2010; Contini et al. 2011; Sanders et al. 2011), such that all these galaxies follow the FMR. In addition, the FMR allowed Mannucci et al. (2011); Campisi et al. (2011), to show that the hosts of t long-GRBs have the same metallicities of the other star-forming galaxies. However, they found some metallicity evolution of the FMR at $z \sim 3.3$, where galaxies tend to have lower metallicities.

All the observational studies mentioned in the previous paragraph refer to the gas-phase metallicity, as measured by emission lines. Gallazzi et al. (2005) presented the local mass-stellar metallicity relation based on ~170 000 SDSS galaxies (Sloan Digital Sky Survey Data Release Two). The stellar metallicities were derived using the Lick system of spectral indices in the optical region which are sensitive to the overall metallicity of the stellar population, primarily dominated by intermediate/old stars. They adopted a Bayesian statistical approach and derived the stellar metallicities by comparing the observed spectrum of each galaxy with a comprehensive library of model spectra corresponding to different star formation histories. They found that at low masses, the stellar metallicity increase with mass, while above $\sim 3 \times 10\ M_{\odot}$ the relation flattens out. In addition they noted that gas-phase metallicity is most reliably for star-forming galaxies, whereas stellar metallicity is best determined for early-type galaxies, and found that the stellar metallicity is generally lower than the gas-phase metallicity (by 0.5 dex). Panter et al. (2008) inferred the stellar metallicity history of SDSS galaxies and determined their stellar mass-stellar metallicity relation. They used a different approach respect to Gallazzi et al. (2005), but they found similar results. Moreover, considering only the younger population of galaxies ($\leq$1 Gyr) they found good agreement also with the gas phase metallicities.

A very limited work has instead been done on stellar metallicity at high redshift, see Shapley (2011) for a review. As in local starbursts, the strongest features in the rest-frame ultraviolet (UV) spectrum of distant galaxies are interstellar and photospheric absorption lines of C, N, O, Si, and Fe, produced by hot, young O-B stars (see Shapley et al. 2003). One advantage in using these spectra to measure the metallicity at $z \sim 3$ is that the UV rest frame is shifted into the optical spectral region, which is easier to observe from ground-based telescopes. However, very high signal-to-noise (S/N) in the stellar continuum is required to study the relevant absorption features for metallicity measurements, therefore these studies have been performed, until now, mainly for either gravitationally lensed galaxies (Rix et al. 2004; Quider et al. 2009; Dessauges-Zavadsky et al. 2010) or co-added star-forming galaxy spectra (Halliday et al. 2008).

Several authors have presented calibrations of stellar metallicity based on UV absorption lines. Leitherer et al. (2001) investigated the influence of metallicity on the spectra of star forming galaxies. In particular, they investigated some blended photospheric lines whose strengths depend only on metallicities. They found that the two blends of lines near λ1370 Å and λ1425 Å (which they attributed to OV λ1371 Å and FeV λ1360–λ1380 Å and to SiIII λ1417 Å, CIII λ1427 Å and FeV λ1430 Å respectively) have equivalent widths that increase steadily with metallicity and do not depend on other stellar parameters, such as age and the IMF. Rix et al. (2004) using the Starburst99 models plus their non-local thermal equilibrium (non-LTE) model atmosphere code WM-basic, supported the conclusions that these lines are useful metallicity indicators, and suggested a new indicator at λ 1978 Å. Rix et al. (2004) applied these new indicators to measure the stellar metallicity of two lensed galaxies, MS 1512-cB58 at $z = 2.73$, and Q1307-BM1163 at $z = 1.411$, finding good agreement with the gas phase metallicity.

On the basis of these studies, Mehlert et al. (2006) calculated the *EW*s of the λ1370 Å λ1425 Å for 12 galaxies with $2.37 < z < 3.40$ in the FORS deep field. They investigated the evolution of the *EW*s and the metallicity with the redshift, and found that the abundances of heavy elements increase with the redshift. Halliday et al. (2008), instead, computed the stellar metallicity using the λ1978 Å indicator for a co-added unlensed star forming galaxy spectra at $z \sim 2$. Comparing their results with the gas phase metallicity of galaxies with similar mass, they found that their stellar metallicities were lower by a factor of ~0.25 dex. Quider et al. (2009) computed the stellar metallicity of the gravitationally lensed galaxy Cosmic Horseshoe at $z = 2.38$ by using the λ1425 Å metallicity indicator, found good agreement between stellar and gas phase metallicity. Quider et al. (2010) carried out a similar study for the lensed galaxy called the Cosmic Eye at $z = 3.07$. Owing to the presence a strong sky lines in the region of the stellar metallicity indicators, these authors were unable to precisely measure the stellar metallicity, but provide only an indication by comparing the observed spectra with the model. Finally, Dessauges-Zavadsky et al. (2010) studied the stellar metallicty for the lensed galaxy 8 o'clock arc at $z = 2.73$. Using the λ1425 Å and λ1978 Å photospheric indices, they found comparable metallicity for the gas and the stellar component.

All these studies provide important constraints on models of galaxy formation. Many models incorporate the processes of gas infall and outflows, and the properties of feedback and galactic winds (Dekel & Woo 2003; Veilleux et al. 2005; Murray et al. 2005; Davé et al. 2007; de Rossi et al. 2007; Brooks et al. 2007; Tornatore et al. 2007; Somerville et al. 2008; Oppenheimer & Davé 2008; Finlator & Davé 2008; Mouhcine et al. 2008; Dayal et al. 2009; Tassis et al. 2008; Kobayashi et al. 2007; Calura et al. 2009; Spitoni et al. 2010; Salvaterra et al. 2011; Sakstein et al. 2011). The lack of evolution in the FMR, the associated evolution of the mass-metallicity relation, and the properties of the effective yields place strong constraint on models. In this picture, the stellar metallicity can be used as an independent measurement to test the predicted metallicity evolution (De Rossi et al. 2007; Davé & Oppenheimer 2007).

In this paper we study the stellar metallicity of a sample of galaxies at $z > 3$. In Sect. 2, we review the different indices used to estimate stellar metallicity at high-z, and define a new rest-frame UV feature suitable for such measurements to enlarge the number of available metallicity indicators. In Sect. 3, we present our sample of high redshift galaxies and compute their stellar metallicity by applying the calibrations found. In Sect. 4, we calculate the stellar and gas phase metallicity for some lensed galaxies found in the literature, and we compare the two. Finally, we present the first stellar mass-stellar metallicity relation obtained at $z > 3$, followed by the conclusions.

2. Stellar metallicity from absorption lines

When studying high-redshift galaxies, it is useful to have a large number of calibrated features over a large wavelength range to increase the constraints on metallicity and avoid the effects of atmospheric absorption bands and bright sky emission lines.

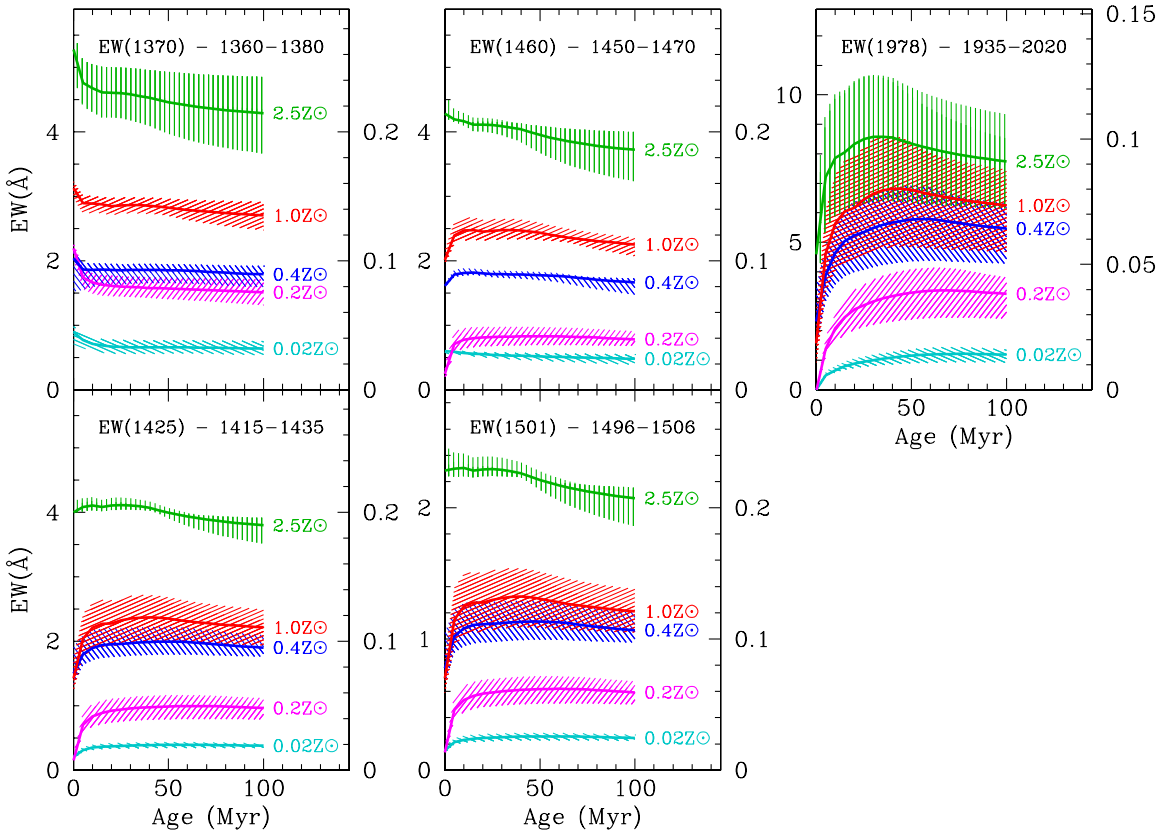

Fig. 1. Variation of the line indices with stellar population age and metallicity. In each plot, the EW is shown in left vertical axis, while the right axis shows the average fractional depth below the continuum. For each feature we draw the models constructed with Starburts99 at five value of metallicity as shown in different colors. For each metallicity, the color regions represent the error due to the dependence on the IMF assumed. In this way we can highlight the dependence of the models and robustness of the indices from the IMF and stellar population age assumed.

A feature can be used as a metallicity indicator if the following conditions are satisfied: 1) the EW is deep enough to be measured in high redshift galaxies; 2) it varies significantly with the metallicity; and 3) it does not depends critically on either age or IMF.

The aim of this work is to update the previous metallicity calibrations and to increase the number of possible indices in UV spectral region. We attempt to measure the stellar metallicities of high redshift galaxies by comparing the observed photospheric lines to model spectra produced using the population synthesis code Starburts99 (Leitherer et al. 1999). The original version of this code allowed the creation of synthetic UV spectra with a variety of ages and IMFs, and used the stellar evolution models to follow the stellar population over time. The first release included only a few different metallicities because empirical stellar libraries were available for only Milky Way O-type stars observed with the International Ultraviolet Explorer (IUE) satellite. Some Galactic B stars were later added to that library by de Mello et al. (2000). To consider the sub-solar heavy element abundances, a new improvement was obtained in 2001 with the inclusion of a library of O-type spectra obtained from HST STIS observations of stars in Large and Small Magellanic Clouds (Leitherer et al. 2001). Rix et al. (2004) followed an other approach by utilizing theoretical library spectra instead of empirical ones. Their purpose was to synthesize the photospheric absorption lines seen in the spectra of star forming galaxies taking into account the effects of non-LTE and stellar winds model atmosphere, and their combined effects on the spectral synthesis of hot stars. They therefore replaced the empirical library with a grid of theoretical spectra generated with the hydrodynamical code WM-basic. The major difference between these two approaches is that the empirical spectra have prominent UV interstellar absorption lines that are not present in the theoretical spectra, which are purely stellar. Nevertheless, the authors found good agreement between the empirical and the theoretical spectra.

Since Rix et al. (2004) in principle focus on photospheric lines, processes such as shock emission that affect only high-ionization stellar-wind lines were not included in their models. These limitations were addressed to some extent in the latest generation of the WM-basic code (Leitherer et al. 2010), which is used in this work. This latest version is optimized to compute the strong P Cygni type lines originating in the wind of the hot stars. This is a significant improvement compared to the use of only faint photospheric lines, because the stellar-wind features are stronger, hence more easily detectable in low S/N spectra.

The models of Starburst99 combined with the WM-basic library allows the creation of simulated spectra depending on a number of free parameters related to star formation history, IMF, age, metallicity, supernova and black hole cut-off, stellar atmospheres and microturbolence. We generated galaxy model spectra using the Padova tracks, by including the effects of thermally pulsing AGB stars, for five values of metallicities, 0.02, 0.4, 0.2, 1.0, and 2.5 $Z_{\odot}$ and assuming continuous star formation histories, as presented in Fig. 1. We considered five different

Table 1. List of the metallicity indicators with the corresponding elements, and regions where the equivalent widths are integrated.

Indicator ID	Element	λ range
F1370	OV, FeV	1360–1380[a]
F1425	CIII, FeV, SiIII	1415–1435[a]
F1460	NiII	1450–1470[b]
F1501	SV	1496–1506[b]
F1978	FeIII	1935–2020[c]

Notes. For an additional indicator at λ1533 we refer to Sect. 2.4. [(a)] Leitherer et al. (2001); [(b)] this work; [(c)] Rix et al. (2004).

stellar initial mass functions (IMF). The reference model was a classical Salpeter power law with an exponent $\alpha = 2.35$ and upper mass limit of $M_{\rm up} = 100\ M_{\odot}$. We also considered two IMFs with $\alpha = 1.85$ and $\alpha = 2.85$ between 1 $M_{\odot}$ and 100 $M_{\odot}$, and another with $\alpha = 2.35$ and a mass limit $M_{\rm up} = 6\ 0 M_{\odot}$. Finally, we computed models for a Kroupa IMF.

2.1. Metallicity indicators

The UV spectrum of star forming galaxies is dominated by strong photospheric absorption features that are sensitive to metallicity.

Leitherer et al. (2001) investigated the existence of some blended photospheric lines whose strengths depend only on metallicity. They found that the two blends of lines near λ1370 and λ1425 (which they attributed to OV λ1371 and FeV λ1360–λ1380 and to λSiIII 1417, CIII λ1427, and FeV λ1430, respectively) have equivalent widths that increase steadily with metallicity and do not depend on other parameters. Rix et al. (2004) agree with previous conclusions that these lines are useful metallicity indicators, and suggested a new robust indicator at $\lambda \sim 1978$ Å.

Here we use the spectra of the new version of Starburst99 to update the calibrations of the aforementioned features and find additional new useful features. Using the new library, our measurements confirm that the indicators proposed in the previous studies, (F1370, F1425, and F1978) are stable after ~30 Myr from the onset of star formation, and increase monotonically with metallicity with a mild dependence on other parameters (see Fig. 1). Previous works have successfully used these indices (Halliday et al. 2008; Quider et al. 2009). The predicted EWs derived using the last version of the Starburst99 code are similar to the previous ones evaluated for the 1425 Å index (0.11 Å at solar metallicity). However, for the 1978 Å index the difference is higher, especially at high metallicity (1.95 Å at solar metallicity). Moreover, the F1978 index is quite sensitive to the assumed IMF (see Fig. 3), which affects its reliability as a metallicity indicator.

2.2. New indicators

The first region that we investigated is that between 1496 Å and 1506 Å. We chose this region because the SV λ1501 line is an absorption feature that originates in the photosphere of the hot stars, as noted by Pettini et al. (1999) and Quider et al. (2009). Figure 1 shows the age stability and the dependence on metallicity of this index: as in previous cases, this line satisfies the necessary conditions for a robust metallicity indicator.

Table 2. Coefficient of the equation $\log(Z/Z_{\odot}) = \alpha + \beta EW + \gamma EW^2$ for each index considering the real continuum.

Index	α	β	γ
F1370	–2.501	1.403	–0.1700
F1425	–2.003	1.203	–0.1521
F1460	–2.023	1.251	–0.1631
F1501	–2.152	2.324	–0.5329
F1978	–2.051	0.388	–0.0122

Table 3. Coefficient of the equation $\log(Z/Z_{\odot}) = \alpha + \beta EW + \gamma EW^2$ for each index, considering the pseudo-continuum.

Index	α	β	γ
F1370	–2.897	2.346	–0.4208
F1425	–2.138	2.116	–0.4424
F1460	–2.183	2.336	–0.5212
F1501	–2.543	4.800	–1.968
F1978	–2.774	1.070	–0.0936

Another region that we considered is that between 1450 Å and 1470 Å. It has never been investigated before whether this region contains some photospheric lines, but we found that the NiII feature at λ1460 has the same dependence on metallicity as the other lines discussed above, where the equivalent width depends strongly on metallicity, but not on either age or IMF.

We therefore defined two new line indices, F1460, and F1501, as the equivalent widths integrated between 1450–1470 Å and 1496–1506 Å, respectively.

The list of the metallicity indicators presented above are reported in Table 1. Figure 2 presents the smoothed and normalized reference models obtained with Starburts99 at metallicities 0.02, 0.4, 0.2, 1, and 2.5 $Z_{\odot}$. The strengths of the absorption features discussed above is clearly a strong and monotonic function of metallicity.

2.3. Metallicity calibrations

To perform an accurate determination of metallicity, we interpolated the relation between the equivalent widths of the indicators as a function of $\log(Z/Z_{\odot})$ discussed above.

We fitted a second-order polynomial to measure the values of the equivalent widths. The results of the fitting are presented in Fig. 3: the triangles represent the reference model (Salpeter IMF with $\alpha = 2.35$ and age = 50 Myr), the black line is the quadratic fit to these models, and the grey region represents the uncertainty in the calibration caused by the different assumed IMF, as shown in Fig. 1. We used a second-order fit expressed as

$$\log(Z/Z_{\odot}) = \alpha + \beta EW + \gamma EW^2 \quad (1)$$

the coefficients for the best-fit relations of five indices are in Table 2.

2.4. The feature SiII at 1533λ

In addition to the two new indicators that we defined , we also studied the SiII λ1533 feature, which is defined as the EWs integrated between 1530 Å and 1537 Å. This line appears to be a robust metallicity indicator: in addition to satisfying the necessary conditions to be a metallicity index, as discussed in Sect. 2.2, this line is far deeper than the others and defined for a narrow wavelength range of 7 Å.

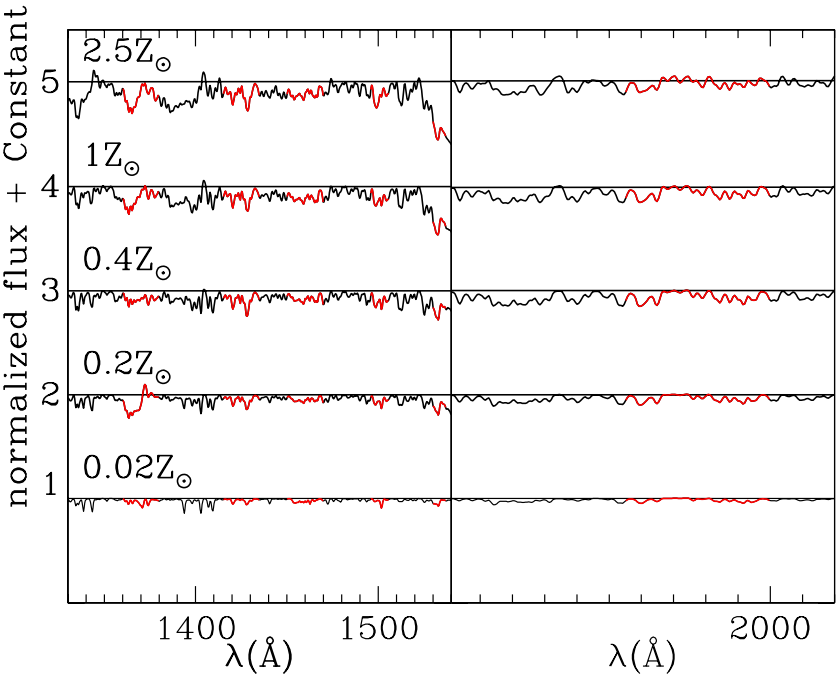

Fig. 2. Smoothed and normalized reference models obtained with Starburts99 for a metallicity of 0.02, 0.4, 0.2, 1, and 2.5 $Z_\odot$. In red we highlight the metallicity indicators discussed in the text to illustrate their dependence on metallicity.

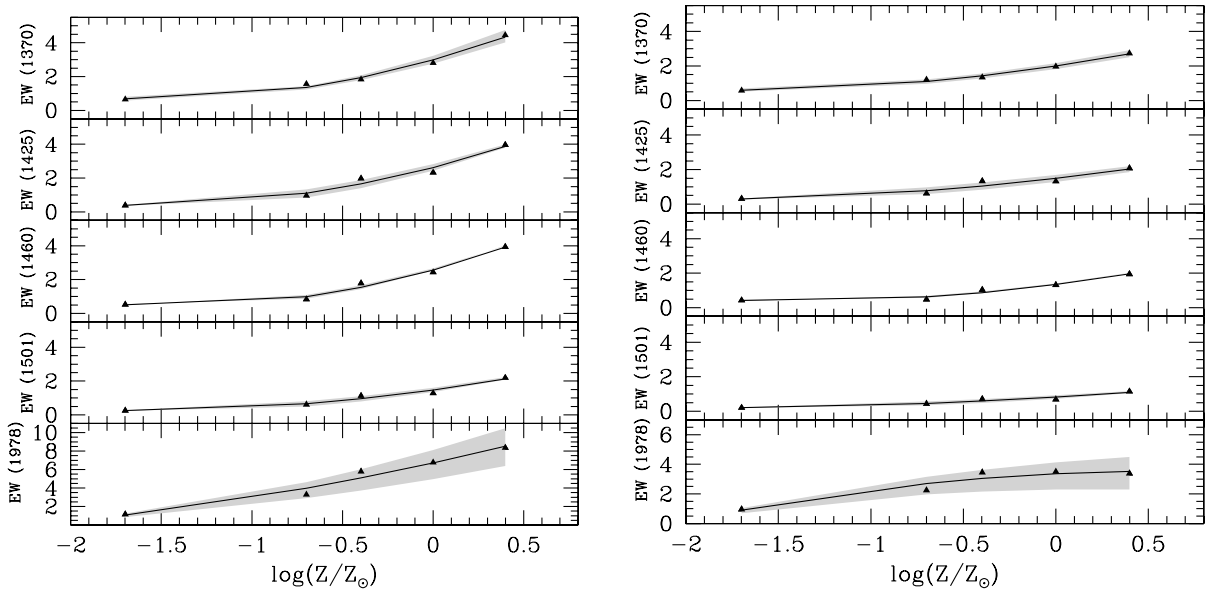

Fig. 3. *EW-Z* relations for the five indices considered. The triangles represent equivalent widths measured from the reference models at age 50 Myr, while the solid line is the quadratic fit given by equations in Table 2 for the real continuum (*left panels*) and Table 3 for the "pseudo-continuum" (*right panels*). The grey region represents the error caused by the dependence of the models on the IMF assumed.

Unfortunately, the SiII line is also often detected in emission: see e.g. the spectrum of very high S/N presented by Shapley et al. (2003). This emission appears to be very weak, and in low resolution spectra it may difficult to recognize. In addition, this is a fine line structure, (Pettini et al. 2004): although this feature is normally photospheric, in dense environments it can be interstellar as well. We therefore recommend that it be used with caution, and only in spectra where emission is either absent or sufficiently weak not to compromise the measurements of the EW.

We nevertheless present the calibrations obtained for this feature, and discuss the results found for the observed galaxies when using it as a metallicity indicator.

The obtained calibrations are:

$$\mathrm{Log}(Z/Z_\odot) = -1.845 + 1.332EW - 0.2077EW^2 \quad (2)$$

in the case of a real continuum, and

$$\mathrm{Log}(Z/Z_\odot) = -1.893 + 1.717EW - 0.339EW^2 \quad (3)$$

in case of a "pseudo-continuum".

The results found using this feature are presented in Sect. 3.4.

2.5. Calibration uncertainties

In previous sections we have defined two new photospheric lines that are sensitive to stellar metallicity and independent of any other stellar parameter (such as age and IMF), centered on ∼1460 Å and ∼1501 Å, and we recalibrate with updated stellar libraries the stellar features at ∼1370 Å ∼1425 Å and ∼1978 Å proposed by Leitherer et al. (2001) and Rix et al. (2004) to derive the stellar metallicity. Both the old and the new metallicity indicators are affected by significant uncertainties.

Starburts99 consider two different cases of star formation: an instantaneous burst and continuous star formation at a constant rate. In the former, the spectrum changes rapidly with time, whereas in the latter the equilibrium is reached after a few Myr, and then the spectrum changes little with time. In the case of a single burst, we expect to observe galaxies for which the O-B stars have already died, whereas for galaxies with a continuous star formation rate the integrated light is dominated by bright and hot massive stars that determine the UV continuum (see Adelberger et al. 2004). We therefore, decided to consider the continuous star formation rate to create models with Starburts99 because it seems to be the most accurate possible description of most star forming galaxies.

Another critical issue in this kind of work is an accurate determination of the continuum level. We note that, unlike in other similar works (see Rix et al. 2004) the values of EW that we measured are relative to the real, theoretical continuum. However, low- and medium-resolution spectra often do not have many spectral regions free of absorption lines, and the estimate of this continuum is not straightforward. In this cases, it is common to define a "pseudo" continuum by fitting a spline curve through the mean flux in some spectral windows that are relatively free of both emission and absorption lines, and producing a normalized spectrum by dividing by this fit. This definition tends to underestimate the real continuum because no spectral window is totally free of absorption, but using the same definition of "pseudo" continuum for both calibrations and observations, this uncertainty tends to cancel out.

When observing faint, high-redshift galaxies, the aformentioned method is difficult to use, because either the spectra have insufficient S/N in the narrow wavelength ranges (1–2 Å, Rix et al. 2004) used to define the "pseudo" continuum, or the bright sky-lines present at $\lambda > 7000$ Å can prevent any robust analysis of these regions. As a consequence, each spectrum needs a specialized recipe to compute the continuum according to the wavelength range covered and the S/N at each point. Since in some cases it is easier to use the "pseudo" continuum (hereafter the former procedure) and in other cases to estimate the real continuum (hereafter the latter procedure), we provide the calibrations derived for both procedures.

In Table 3, we provide the coefficients for the calibrations based on the definition of the "pseudo-continuum" of Rix et al. (2004) (see Table 3 in their paper for the regions used to define the continuum), the former set of calibrations which are based on the last version of Starburts99. Figure 3 (right panel) displays the relations obtained between metallicity and EW.

A side effect of these two different procedures is that these calibrations have no or a very weak dependence on spectral resolution, which is high enough to well sample the region of interest, i.e., 10 Å rest-frame. Only the F1978 index depends strongly on resolution, as already noted by Halliday et al. (2008). In addition, this index also depends on the IMF, as shown in Fig. 3.

We emphasize that the former set of calibrations are more easy to use because the definition of the "pseudo continuum" is unambiguous: only some tiny and defined regions are used to defined the "pseudo continuum", and not the entire continuum, as for the latter set. Therefore, we recommend use of the "pseudo continuum" in case of spectra of high S/N, where the continuum is less affected by bright sky lines and emission or absorption interstellar lines, and in case of spectra of low S/N we suggest the use of the former set of relations and define the real continuum for each spectrum to select regions unaffected by strong, bright sky lines.

3. Stellar metallicity in high redshift galaxies in the AMAZE sample

Now we describe how we applied the method and the relations presented above to a sample of five galaxies at $z \sim 3.3$ to determine, for the first, the stellar mass- stellar metallicity relation at this redshift.

3.1. Observations

For the present investigation, we selected a sub-sample of AMAZE galaxies at $z \sim 3.3$ for which gas metallicities and stellar masses had already been accurately measured by Maiolino et al. (2008) and Trocoso et al. (in prep.) see Table 4. The masses presented in Table 4 differ slightly from those presented in Maiolino et al. (2008) because the calculation was improved by using new Spitzer IRAC photometry available. The observed galaxies were originally selected from the GOODS-MUSIC sample (Grazian et al. 2006), and are all in the same field allowing for multi-object spectroscopy.

Observations of the galaxies were obtained in service mode in three runs (Nov.–Dec. 2008, Nov.–Dec. 2009, and Sept.–Dec. 2010) using FORS2 (FOcal Reduced and low dispersion Spectrograph 2, Appenzeller et al. 1992) at the ESO VLT (UT4), under seeing conditions of about 0.8 for each run. The extended multi-object mode (MXU) was used to optimize the number and placement of targets in the masks and ensure that a homogeneous sample of observations were carried out using a standardized set-up. The slit width was equally set to 1 arcsec, corresponding approximately to the size of typical high-redshift galaxies under the average atmospheric conditions at Paranal. For all observations, the low resolution grism 300I was used. This grism covers a range of CCD sensitivities (6000−11 000 Å) with a relatively high efficiency, reaching its maximum at around 8600 Å. The total exposure time was 37 h.

3.2. Data reduction

The data reduction was performed using the ESO FORS-pipeline. The default reduction procedure for these spectroscopic science data is as follows. The data are first corrected for bias, then an extracted mask, containing the positions of the long slit and the spatial curvatures of the spectra, is applied to the science data. The data are then flat-fielded and re-mapped eliminating the effect of cosmic-ray hits and the optical distortions. Afterwards, they are rebinned to constant wavelength steps. The wavelength calibration is adjusted using sky emission lines, allowing corrections to be made for shifts between night-time science and day-time calibration data.

The sky background is obtained using a median of the pixel free from emission lines, and the sky is subtracted before remapping, i.e. when the spectra are still in the original CCD coordinate system. The sky is determined with a robust linear

Table 4. Properties of objects observed with FORS.

ID	RA(J2000)	Dec(J2000)	$R_{\rm mag}$	z	SNR^a	Log$M$	12 + Log(O/H)$_{\rm gas}$
CDFS-12631	03 32 18.1	–27 45 19.0	24.72	3.709	7	$9.84^{+0.15}_{-0.07}$	$8.22^{+0.18\,b}_{-0.14}$
CDFS-9313	03 32 17.2	–27 47 54.4	24.82	3.654	8	$9.34^{+0.17}_{-0.23}$	$7.95^{+0.25\,b}_{-0.23}$
CDFS-6664	03 32 33.3	–27 50 07.4	24.80	3.797	8	$8.98^{+0.20}_{-0.09}$	$7.63^{+0.38\,c}_{-0.29}$
CDFS-5161	03 32 22.6	–27 51 18.0	24.96	3.660	4	$9.73^{+0.22}_{-0.23}$	$7.69^{+0.23\,b}_{-0.38}$
CDFS-4417	03 32 23.3	–27 51 56.8	23.42	3.473	14	$10.38^{+0.15}_{-0.04}$	$8.55^{+0.09\,c}_{-0.10}$

Notes. Column 1 object name in the MUSIC catalog (Grazian et al. 2006), Cols. 2, 3: coordinates (J2000), Col. 4: R-band magnitude, Col. 5: spectroscopic redshift, Col. 6: S/N, Col. 7: stellar mass and Col. 8: gas metallicity. $^{(a)}$ Signal-to-noise ratio in the wavelength range used. $^{(b)}$ Troncoso et al. (in prep.); $^{(c)}$ Maiolino et al. (2008).

fitting, which allows for a linear spatial gradient in the background.

For our particular data redaction, flux calibration is performed using spectra of spectrophotometric standard stars obtained each night. These spectra are reduced with the data reduction pipeline, as for the science data, and used to convert the ADUs into flux units. In general, the observed spectra of the standard stars is divided by the corresponding stellar spectra taken from the literature to obtain response curves and calibration factors. Representative correction curves is then created for each run by combining the individual response curves and smoothing the result by a spline interpolation. We finally applied the correction curves and calibration factor obtained to all the observed spectra.

At the end, we obtain 120 flux calibrated spectra for each galaxy.

We combine all the reduced data and finally use the IRAF[1] task apall, with the aperture size of five pixels, to extract one-dimensional spectra for the objects. The list of the sample of galaxies selected for this project are listed in Table 4. The table lists the properties of the objects: ID, RA, Dec, R magnitude, spectroscopic redshift, S/N of the summed spectra, stellar mass, and gas phase metallicity.

Because of the low S/N of some reduced data, we could not use all the spectra for our analysis. After a careful visual inspection, we removed from our sample the galaxy CDFS-5161 because its spectrum presents too low a S/N to detect the single lines. Moreover, we combined the three galaxies CDFS-12361, CDFS-9313, and CDFS-6664 to increase the signal of the individual spectra (hereafter we call it CDFS-comb spectrum). The spectrum of the CDFS-4417 galaxy was of sufficient high S/N to be used individually.

3.3. Continuum levels and EWs

Defining the continuum is a critical step in measuring the EWs. First, the S/N of our spectra is generally limited (see Table 4) and changes significantly with wavelength because of the presence of sky-lines. Second, at our resolution most of the spectrum is affected by absorption lines. Taking into account these two problems, we fitted the continuum by using a third- or fifth-order polynomial, depending on the continuum shape, by using only regions that are expected to be free from strong absorption lines. To define the continuum, we used the Starburst99 spectra, excluding all the regions where absorption larger than 5% is expected for solar metallicities. This method defines a continuum that is slightly underestimated. The amount of correction needed can be measured by applying the same technique to theoretical spectra, where the continuum level can be reliably determined. We found that our fitting method defines a continuum level that is 3 ± 2% below the real one, depending on the spectrum used. This means that the continuum bias can be removed by multiplying the normalized spectra by 1.03. A series of simulations were also used to estimate the uncertainties in the continuum level for each target galaxy. Random Gaussian noise was added to the Starburst99 spectra to ensure the same S/N in each spectrum, and the continuum was fitted, repeating the procedure many times. We found that the continuum level is uncertain by about 5% for CDFS-4417, and 10% for the combined spectrum, and that this uncertainty is fairly constant with wavelength.

The EW are measured with respect to this fitted continuum, after excluding regions affected by bright sky lines. The uncertainties in the EWs derived from both the poisson noise in the used pixels, and the uncertainties in the continuum level described above. The latter type of uncertainty is dominant in all cases, and can become very large for F1978 which is 85 Å wide. In contrast, F1501 index is defined for the narrowest of all the indices wavelength range and is less affected by this contribution. As a result, F1501 is usually the most reliable index for our galaxies.

3.4. Results

The EWs measured as described above are compared with the calibrations in Table 2 to obtain the stellar metallicities. We consider neither F1370, which is unmeasurable in our spectra of limited signal-to-noise, nor F1978, which, for our redshifts, falls in wavelength regions covered by many sky lines. Therefore for the observed galaxies we are able to use only F1425, F1460, and F1501.

Figures 4 and 5 compare both the observed spectrum of CDFS-4417 (solid line) and the composite spectrum CDFS-comb (solid line) with the theoretical models (dotted line), computed for five different metallicities for the indices considered to compute the stellar metallicity. Among the five models plotted in the figures, the metallicities that most closely match the observations are 0.2 $Z_\odot$, in all the spectra.

This agreement can be verified more quantitatively by using the equations reported in Table 2 and computing the metallicity for the observed objects. In Table 5 we present the value found for each available features and its associated error calculated applying the theory of the propagation of errors, i.e. we propagated the uncertainties both in the observations and the models to get the final value. The last column of Table 5 provides the final

[1] IRAF (Image Reduction and Analysis Facility) is distributed by the National Optical Astronomy Observatories, which are operated by the Association of Universities for Research in Astronomy, Inc., under cooperative agreement with the National Science Foundation.

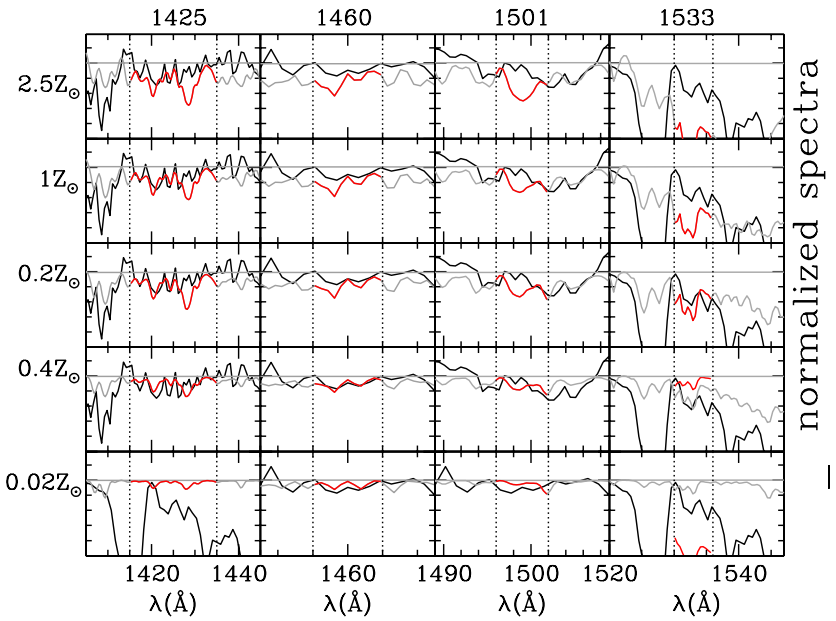

Fig. 4. Comparison of the observed spectrum of the object CDFS-4417 at $z = 3.47$ (black line) with the theoretical spectra (dotted grey line) produced by Starburts99 for five different metallicities and for each index used to compute the stellar metallicity. In red we highlight the metallicity indicators. All the spectra are normalized by the fitted continuum.

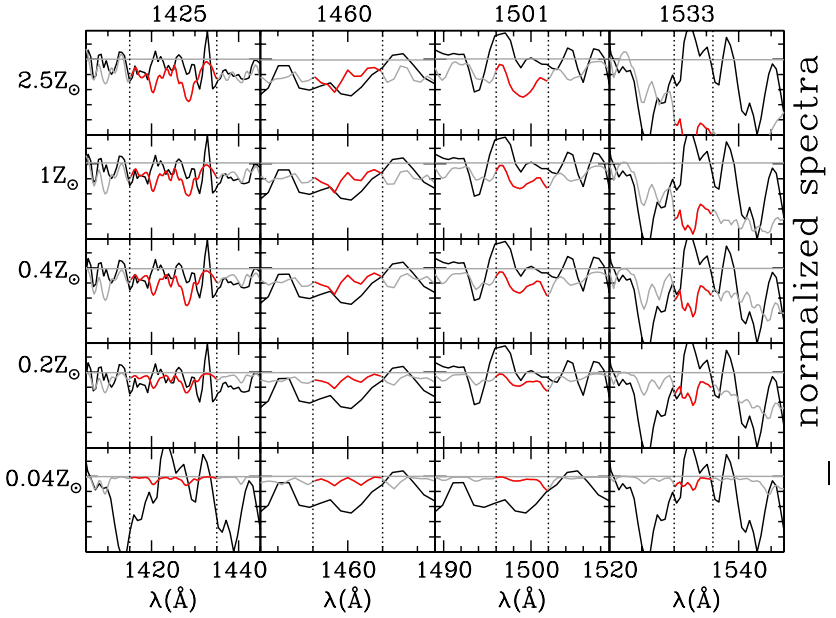

Fig. 5. Comparison of the observed combined spectrum of the object CDFS-comb at $z = 3.71$ (black line) with the theoretical spectra (dotted grey line) produced by Starburts99 for five different metallicities and for t each index used to compute the stellar metallicity. In red we highlight the metallicity indicators. All the spectra are normalized by the fitted continuum.

value of metallicity evaluated to be the weighted average of the metallicities for the single features and the associated weighted error.

Since in our spectra we did not detect any emission at 1533λ, we calculated the metallicity of the spectrum CDFS-4417 by applying Eq. (2), and we found a value of $Z = 0.26\,Z_{\odot} \pm 0.12$. This value is in good agreement with that found using the other indicators (0.23 ± 0.22), and the associated formal error is smaller. This suggests that it is possible to use the SiII line at 1533λ as a metallicity indicator when the spectra is free from the Si II* fine-structure emission line. The final value of the stellar metallicity does not change even when we instead compute the weighted average using also this feature, where possible.

The gas phase metallicity of the CDFS-4417 was taken from Maiolino et al. (2008), while for the combined FORS spectrum we combined the rest-frame optical spectrum in the same way as we did for the rest frame UV one, to derive consistent properties. We measured the gas phase metallicity with the R_{23} parameter using the line fluxes measured in the combined spectrum.

4. Other data from literature

To enlarge our data set we collected from the literature other rest-frame UV spectra suitable for this kind of work.

To compute the gas-phase metallicity we adopted one of the most frequently used metallicity diagnostics, the R_{23} parameter, defined as:

$$R_{23} = \frac{F([\mathrm{OII}]\lambda 3727) + F([\mathrm{OIII}]\lambda 4959 + F([\mathrm{OIII}]\lambda 5007)}{F(\mathrm{H}_{\beta}\lambda 4861)}$$

where F([O II]λ3727), F([O III]λ4959), and so on denote the emission-line fluxes of [O II]λ 3727, [O III]λ4959, and so

Table 5. Metallicity measured in the observed galaxies with the errors computed using all the available indicator, and weighted average.

ID	F1425	F1460	F1501	Weighted average
CDFS-4417	0.14 ± 0.44	0.17 ± 0.47	0.30 ± 0.32	0.23 ± 0.22
CDFS-comb	0.13±0.74	0.37 ± 0.62	–	0.24 ± 0.45

on, respectively. The R_{23} parameter was proposed by Pagel et al. (1979), and its relation to the oxygen abundance has been improved by using both photoionization model calculations (e.g., McGaugh 1991; Kewley & Dopita 2002), and empirical calibrations (Nagao et al. 2006). For consistency with the FORS galaxies discussed above, and to compare with the data of Mannucci et al. (2010), we used the most recent R_{23} calibration provided by Maiolino et al. (2008).

4.1. The Cosmic Horseshoe

The spectrum of Cosmic Horseshoe, a gravitationally lensed galaxy at $z = 2.38$, was analyzed by Quider et al. (2009). They measured the EW of the F1425 index and following the definition obtained a metallicity $Z = 0.5\ Z_\odot$. Their value of EW was obtained by considering the pseudo continuum as defined in Rix et al. (2004). To be able to compare the Cosmic Horseshoe metallicity with those of other galaxies, we measured the EWs using the definition of the real continuum described in Sect. 3.3, and computing the metallicity with Eq. (1). With our procedure, the metallicity that we found is $Z = 0.37\ Z_\odot$, i.e. $12 + \log(\mathrm{O/H}) = 8.26 \pm 029$.

For consistency, we recomputed the gas phase metallicity of these galaxies using the R_{23} index for the emission line fluxes of Hainline et al. (2009) and the metallicity calibration of Maiolino et al. (2008). In this way, we obtained $12+\log(\mathrm{O/H}) = 8.48\pm0.1$.

We measured, for the first time, the stellar mass of the Cosmic Horseshoe. We obtained the IRAC photometry at 3.6 μm and 4.5 μm by using Spitzer archive images and using a photometric aperture of 8 arcsec and subtracting the flux from the central lensing galaxy. The U, G, and I photometry were taken from Belokurov et al. (2007). We used the Hyperzmass code (Pozzetti et al. 2007; Bolzanella et al. 2000) with Bruzual & Charlot (2003) libraries, assuming a Chabrier IMF (Chabrier et al. 2003) with an upper mass limit of 100 $M_\odot$, smooth exponentially decreasing star formation histories (SFHs) with time scale $\tau = [0.1, \infty]$ and age $t = [0.1, 20]$, deriving a mass of $\log(M/M_\odot) = 10.56 \pm 0.19$, after correcting for the magnification.

4.2. The Cosmic Eye

The lensed galaxy Cosmic Eye at $z = 3.075$, was studied by Quider et al. (2010). They did not use the method explained by Rix et al. (2004) to compute the metallicity because of the heavy contamination of absorption lines in the region of the F1425 index that can affect the accuracy of the determination of the continuum. Instead, they just gave an indication of the metallicity, $Z \sim 0.40\ Z_\odot$, by comparing the observed spectrum with the models. Computing the EW of the other indices and applying our calibration, we found a metallicity of $Z = 0.30\ Z_\odot$, i.e. $12 + \log(\mathrm{O/H}) = 8.36 \pm 0.20$.

We computed the gas phase metallicity to be $12+\log(\mathrm{O/H}) = 8.60 \pm 0.11$, by taking the value of R_{23} from Stark et al. (2008) and applying it to the metallicity calibrations of Maiolino et al. (2008).

The stellar mass of the Cosmic Eye derived from SED fitting is $\log(M/M_\odot) = 9.55 \pm 0.14$ (Troncoso et al., in prep.).

4.3. MS 1512-cB58

The last target for which we obtained a spectrum was MS 1512-cB58 (Pettini et al. 2000), a gravitational lensed galaxies at $z = 2.72$ that, thanks to its magnification, has a spectrum of very high S/N. As for the previous galaxies, we measured the EWs of all the defined indicators in the spectra using the real continuum and obtained a stellar metallicity from Eq. (1) of $Z = 0.44\ Z_\odot$, i.e. $12 + \log(\mathrm{O/H}) = 8.33 \pm 0.25$.

To compute the gas phase metallicity, we considered the emission line fluxes of Teplitz et al. (2000), and applied the R_{23} calibration of Maiolino et al. (2008), to derive a value of $12 + \log(\mathrm{O/H}) = 8.35 \pm 0.15$.

The stellar mass of MS 1512-cB58 is $\log(M/M_\odot) = 8.94 \pm 0.15$ (Siana et al. 2008).

4.4. Other galaxies

For five additional high redshift galaxies we did not obtain spectra, but only the value of the EWs from the literature. This is the case for the lensed galaxy 8 o'clock arc at $z = 2.73$ studied by Dessauges-Zavadsky et al. (2010), as well as for the four galaxies of the FORS Deep Field with redshift $2.3 < z < 3.5$ presented in Mehlert et al. (2006). Both these papers provide the F1425 index, as defined by Rix et al. (2004), based on the "pseudo continuum".

For the lensed galaxy 8 o'clock arc, we found that the stellar metallicity is $Z = 0.52\ Z_\odot$, i.e. $12 + \log(\mathrm{O/H}) = 8.40$.

Again, to be consistent with the other results, the gas phase metallicity was computed with the R_{23} index with the emission line fluxes taken from Finkelstein et al. (2009) and using the calibrations of Maiolino et al. (2008). We obtained $12+\log(\mathrm{O/H}) = 8.48 \pm 0.1$.

The stellar mass of this galaxy is $\log(M/M_\odot) = 10.25^{+2.22}_{-0.68}$ (Richard et al. 2011). We are unable to provide the errors in the stellar metallicity of this galaxy because Dessauges-Zavadsky et al. (2010) did not give any indication of the uncertainties in EWs.

In the same way, we calculated the stellar metallicity for four FORS Deep Field galaxies studied by Mehlert et al. (2006). We were unable to compute the gas phase metallicity because the emission line fluxes for these galaxies are unavailable. We reported the results in Fig. 7, where we highlighted these objects with black crosses. The masses of these galaxies were provided by Drory et al. (2005, and priv. comm.).

5. Comparison between stellar and gas-phase metallicities

We now compare the stellar metallicity obtained using the empirical calibrations described above with the gas phase ones.

Table 6. Comparison between the stellar metallicity obtained with this work and gas phase metallicity.

ID	Mass	Redshift	Stellar metallicity	Gas metallicity
CDFS-4417	10.38	3.47	8.05 ± 0.22	8.46 ± 0.11^{a}
CDFS-comb	9.38	3.71	7.92 ± 0.24	7.98 ± 0.15^{b}
horseshoe	10.56	2.37	8.26 ± 0.29	8.48 ± 0.11^{c}
8oclock	10.25	2.73	$8.40 - --$	8.42 ± 0.10^{d}
Cosmic eye	9.60	3.07	8.36 ± 0.20	$8.60 - --^{b}$
MS 1525 cB58	8.94	2.72	8.33 ± 0.25	8.35 ± 0.15^{e}
FDF-3173	9.96	3.27	$8.54 - --$	$- - - - - - - -$
FDF-3810	10.95	2.37	$8.90 - --$	$- - - - - - - -$
FDF-5903	11.01	2.77	$8.24 - --$	$- - - - - - - -$
FDF-6934	11.31	2.44	$8.57 - --$	$- - - - - - - -$

Notes. In all the cases we assume a solar value of $\log(Z/Z_{\odot}) = 12 + \log(\mathrm{O/H}) - 8.69$. The mass is given in units of $\log(M/M_{\odot})$. The gas metallicity was calculated using the calibration of Maiolino et al. (2008), and the emission line fluxes taken from [(a)] Maiolino et al. (2008), [(b)] Troncoso et al. (in prep.), [(c)] Hainline et al. (2009), [(d)] Finkelstein et al. (2009), [(e)] Teplitzt al. (2000). respectively.

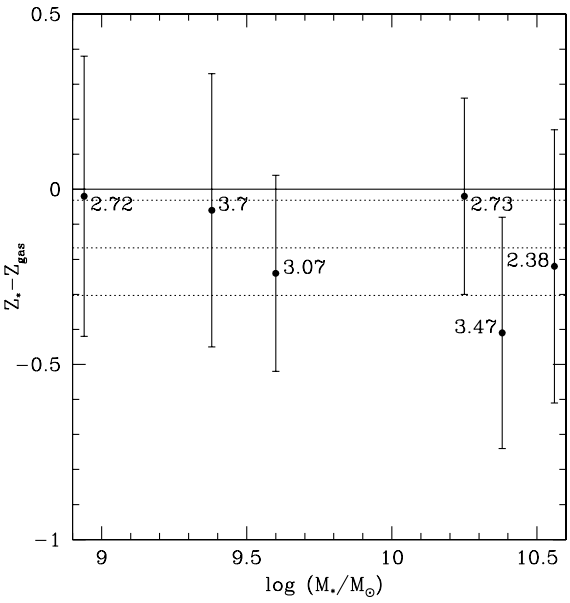

Fig. 6. Difference between the stellar and the gas-phase metallicity of the galaxies. The redshift of each source is reported in the labels. The dotted lines are the mean value of the differences and the 1-σ deviation.

Small differences are expected between the stellar metallicities measured using UV absorption features and the gas phase metallicities obtained by strong optical emission lines. Nevertheless, if the galaxy undergoes rapid metallicity evolution, any differences could be related to the longer lifetimes of the stars dominating the UV emission with respect to the more massive stars dominating the line emission. The stars responsible of the UV emission are indeed young, hot O-B stars (with life times of $\sim 10^6$–10^7 yr), which were formed from interstellar gas with very similar properties to those inferred from emission lines given their short lifetime.

However, larger differences are expected using optical absorption features, which are dominated by the light of longer lived stars (e.g. the Lick indices, as found in Gallazzi et al. 2005; and Panter et al. 2008 for local SDSS galaxies).

In Table 6, we compare the stellar and gas phase metallicities for the objects that we have discussed in the previous sections. The differences between the stellar and the gas-phase metallicities are plotted in Fig. 6. For each galaxy the error were computed by combining the errors in the gas-phase and stellar metallicities in quadrature.

As expected, we do not find a large discrepancy between the two quantities: the average difference is −0.16 and the uncertainty is 0.14, hence the difference is significant at level of about 1.1σ. This does not allow us to claim that there are indeed any significant differences, given the large systematic uncertainties associated with both methods. We note that Halliday et al. (2008), when analyzing star forming galaxies at $z \sim 2$, also found the stellar metallicity to be lower by ∼0.25 dex than the gas phase one measured for a galaxy of similar stellar mass and redshift. Since Halliday et al. (2008) did not compare the metallicities of the same galaxies, some selection effects present in one or both data sets could affect the results. To verify whether there is any difference, we clearly need to analyze data set for a far larger sample of galaxies.

6. The stellar mass-stellar metallicity relation

For the first time our data allow the study of the stellar mass-stellar metallicity relation at high redshift.

Figure 7 shows the position and the relative error for the observed galaxies (black squares) at $z > 3$ presented above in the MZ-plane. The black triangles represent the stellar metallicity for the lensed galaxies. The black crosses are the stellar metallicity calculated for galaxies at $z \sim 3$ taken by Mehlert et al. (2006). All the quantities were computed in the same way and are consistent.

To compare our finding with the previous studies, in Fig. 7 we draw the various mass-metallicity relations found at different redshifts for both stellar and gas phase metallicity. For the latter, the black dotted line is the relation obtained by Tremonti et al. (2004) in the local universe as derived from SDSS data, at $z \sim 0.07$, the magenta dotted line represents the relation obtained by Erb et al. (2006) at $z \sim 2.2$, and the blue dotted line shows the behavior of this relation inferred from the initial sample of LSD and AMAZE sources at $z \sim 3$ by Mannucci et al. (2009).

The green dotted line in Fig. 7 represents the stellar metallicity relation found by Panter et al. (2008) for local SDSS galaxies.

As discussed in the previous section, the derived stellar metallicities are consistent, although slightly lower, than the gas phase ones. The stellar metallicities therefore provide an independent test of the reliability of metal abundance determination for high redshift galaxies, which are more often obtained for only the gas phase using strong optical emission line ratios. However, the gas-phase strong line diagnostics used are indirect tracers that have been calibrated in local galaxies, and depend not only on metallicity, but also on other parameters such

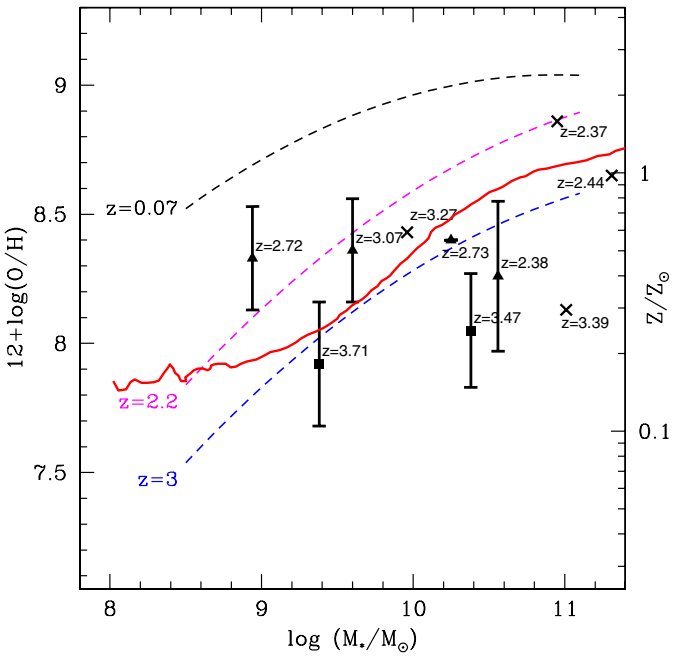

Fig. 7. Stellar mass-stellar metallicity relation for the FORS galaxies at $z \sim 3.3$ discussed in this work (black squares). The black triangles represent the stellar metallicity for the lensed galaxies from the literature (see text), and the black crosses are the stellar metallicity for the galaxies at $z \sim 3$ taken by Mehelert et al. (2006). For comparison, we draw the mass-metallicity relations for the gas component: the black line is the MZR obtained by Tremonti et al. (2004) at $z = 0.07$, the magenta line was found by Erb et al. (2006) at $z = 2, 2$, and the blue dotted line shows the relation from the LSD and AMAZE inferred by Mannucci et al. (2009) at $z \sim 3.5$. The red line is stellar mass-stellar metallicity relation found by Panter et al. (2008) in local universe.

as ionization conditions and densities, which might in principle be very different in high-z star forming galaxies than in local spirals (see e.g. Nagao et al. 2006; Brinchmann et al. 2008). Our result therefore confirms the low chemical abundances derived from optical line ratios at high redshift, and the strong evolution both in gas phase and young star metallicity relative to local and lower redshift galaxies, as previously claimed by Maiolino et al. (2008) and Mannucci et al. (2009). Despite the large uncertainties in both stellar and gas-phase metallicity measurements, this result is consistent wiht the findings of Mannucci et al. (2010) and Troncoso et al. (in prep.) that the fundamental metallicity relation between mass, metallicity, and SFR continue to evolve at $z \sim 3$, while no evolution has been found at lower redshifts (see also Cresci et al. 2012).

As shown in Fig. 6, the stellar metallicities derived for $z \sim 3$ galaxies are comparable to those obtained by Gallazzi et al. (2005) and Panter et al. (2008) for local SDSS galaxies. However, the stellar populations that dominate the spectral features considered in the two cases to compute the metallicity are different. In high redshift galaxies, the rest-frame UV spectrum that we observe is dominated by hot, young stellar populations, while in the local universe the optical indices used by Panter et al. (2008) are dominated by cold, older stars. As noted by Panter et al. (2008), the stellar metallicities of galaxies with a younger stellar populations ($\leq$1 Gyr) are in closer agreement with the gas phase ones, while larger differences are found for galaxies dominated by an older population, hence, a direct, straightforward comparison of the two is impossible. However, the fact that the stellar metallicities of the SDSS sample are comparable to both the gas phase and stellar abundances measured at $z > 2.5$ is an indication that the bulk of the stellar populations in the galaxies investigated by Panter et al. (2008) were formed during this epoch.

7. Conclusions

We have investigated for the first time the stellar mass- stellar metallicity relation at high redshift, $z \sim 3$. Using the theoretical spectra created with the population synthesis code Starburts99, we have searched for photospheric absorption lines that can be used as robust indicators of stellar metallicity.

We first reanalyzed the line indices previously proposed by Leitherer et al. (2001) and Rix et al. (2004), the F1370, F1425 and F1978 using the last version of Starburts99, although the F1978 index depends strongly on both the resolution and the IMF.

We then defined two new photospheric lines, F1460 and F1501, and we found that these lines are sensitive to the metallicity and almost independent of the age and the IMF, and therefore useful stellar metallicity indicators. The F1501 index seems to be the most promising metallicity indicator because it is defined for the narrowest wavelength range and less affected by the uncertainties in the continuum definition.

We provided the metallicity calibrations, which are reproduced in Fig. 3, with two different definitions of the continuum: the first relations have been provided relative to the real continuum, which we suggest be used in the case of spectra of low signal-to-noise ratio, the others were obtained using the definition of the "pseudo-continuum" provided by Rix et al. (2004), which we recommend in the case of high signal-to-noise spectra, as discussed in Sect. 2.3.

We applied the relations to one galaxy and composite spectra comprised of three additional galaxies of the AMAZE sample at $z \sim 3.3$, for which the gas phase metallicity and the galaxy masses were already know.

We took from the literature the spectra of eight additional galaxies, and we recomputed their stellar metallicity using the new calibrations.

At the end, we compared the results found with the gas phase metallicity for each object, as shown in Fig. 6. The main conclusion of our paper is that within the errors, the stellar and the gas phase metallicity are consistent, although we appear to measure a lower stellar metallicity than the gas phase one by ~0.1 dex, as previously found by Halliday et al. (2008). This result supports the evidence of a low metal content derived for the gas phase of high-z galaxies from optical strong line ratios, as well as any evolution in the Fundamental Metallicity Relation at $z > 3$ as found by Mannucci et al. (2010).

For the first time, we obtained the stellar mass-stellar metallicity at redshift $z > 2.5$, as shown in Fig. 7. We note that the stellar metallicities found at high redshift is comparable to those found by Panter et al. (2008) for local galaxies, although the two cannot be easily compared because in high redshift galaxies the stellar metallicity is computed for hot, young stars, while in the local galaxies for older stellar populations.

In summary, the rest-frame UV is rich in metallicity-dependent features, which are able to provide a measure of stellar metallicity in high redshift galaxies. This represents an independent measure of the chemical abundances in galaxies from to the more widespread gas phase metallicities, which can provide tighter constraints on the star formation histories of galaxies in the early Universe. Although this technique is currently limited

to very bright or lensed galaxies with data of sufficiently high S/N, the advent of the next generation of telescopes will provide us much higher quality spectra for high redshift galaxies, and the stellar metallicity indicators will play a more important role in chemical abundances studies at high redshift.

Acknowledgements. G.C. acknowledges financial support from ASI-INAF grant I/009/10/0. We would like to thank Chuck Steidel for kindly providing his spectrum of MS1512-cB58, and Alice Shapley for her spectra of some lensed galaxies. We thank Max Pettini, Claus Litherer and Federico Biondi for useful comments and suggestions. We are grateful to Niv Drory for providing the masses of the FDF galaxies.

References

Adelberger, K. L., Steidel, C. C., Shapley, A. E., et al. 2004, ApJ, 607, 226
Appenzeller, I., Duensing, K. H., Fricke, K., et al. 1992, ESOC, 42, 577
Belokurov, V., Evans, N. W., Moiseev, A., et al. 2007, ApJ, 671, 9
Bolzonella, M., Miralles, J.-M., & Pelló, R. 2000, A&A, 363, 476
Bresolin, F., Pietrzynski, G., Urbaneja, M. A., et al. 2006, ApJ, 648, 1007
Brinchmann, J., Pettini, M., & Charlot, S. 2008, MNRAS, 385, 769
Brooks A. M., Govervato F.,Booth C. M., et al. 2007, ApJ, 655, L17
Bruzual, G., & Charlot, S. 2003, MNRAS, 344, 1000
Calura, F., Pipino, A., Chiappini, C., Matteucci, F., & Maiolino, R. 2009, A&A, 504, 373
Campisi, M. A., Tapparello, C., Salvaterra, R., Mannucci, F., & Colpi, M. 2011, MNRAS, 417, 1013
Chabrier, G. 2003, ApJ, 586, 133
Cresci, G., Mannucci, F., Maiolino, R., et al. 2010, Nature, 467, 811
Cresci, G., Mannucci, F., Sommariva, V., et al. 2012, MNRAS, in press [arXiv:1110.4408]
Contini, T., Epinat, B., Queyrel, J., et al. 2011, in Tracing the Ancestry of Galaxies (on the land of our ancestors), Proc. International Astronomical Union, IAU Symp., 277, 134
Dayal, P., Ferrara, A., Saro, A., et al. 2009, MNRAS, 400, 2000
Davé, R., Finlator, K., & Oppenheimer, B. D. 2007, EAS, 24, 183
Davé, R., Finlator, K., & Oppenheimer, B. D. 2011, MNRAS, 416, 135
Dessauges-Zavadsky, M., D'Odorico, S., Schaerer, D., et al. 2010, A&A, 510, A26
Dekel, A., & Woo, J. 2003, MNRAS, 344, 1131
de Mello, D. F., Leitherer, C., & Heckman, T. M. 2000, ApJ, 530, 251
de Rossi, M. E., Tissera, P. B., & Scannapieco, C. 2007, MNRAS, 374, 323
Drory, N., Salvato, M., Gabasch, A., et al. 2005, ApJ, 619, 131
Ellison, S. L., Patton, D. R., Simard, L., & McConnachie, A. W. 2008, ApJ, 672, L107
Erb, D. K. 2008, ApJ, 674, 151
Erb, D. K., Steidel, C. C., Shapley, A. E., et al. 2006, ApJ, 646, 107
Erb, D. K., Pettini, M., Shapley, A. E., et al. 2010, ApJ, 719, 1168
Feulner, G., Gabasch, A., Salvato, M., et al. 2005, ApJ, 633, L9
Finlator, K., & Dav, R. 2008, MNRAS, 385, 2181
Finkelstein, S. L., Papovich, C., Rudnick, G., et al. 2009, ApJ, 700, 376
Gallazzi, A., Charlot, S., Brinchmann, J., & White, S. D. M. 2005, MNRAS, 362, 41
Garnett, D. R. 2002, ApJ, 581, 1019
Garnett, D. R., Kennicutt, R. C., & Bresolin, F. 2004, ApJ, 607L, 21
Grazian, A., Fontana, A., de Santis, C., et al. 2006, A&A, 449, 951
Hainline, K. N., Shapley, A. E., Kornei, K. A., et al. 2009, ApJ, 701, 52
Halliday, C., Daddi, E., Cimatti, A., et al. 2008, A&A, 479, 417
Juneau, S., Glazebrook, K., Crampton, D., et al. 2005, ApJ, 619, L135
Kewley, L. J., & Dopita, M. A. 2002, ApJ, 201, 1406
Kewley, L. J., & Ellison, S. L. 2008, ApJ, 681, 1183
Kobulnicky, H. A., & Skillman, E. D. 1996, ApJ, 471, 211
Koppen, J., Weidner, C., & Kroupa, P. 2007, MNRAS, 375, 673
Kobayashi C., Springel V., & White S. D. M. 2007, MNRAS, 376, 1465
Leitherer, C., & Heckman, T. M. 1995, ApJS, 96, 9L
Leitherer, C., Schaerer, D., Goldader, J. D., et al. 1999, ApJ, 123, 3
Leitherer, C., Leo, J. R. S., Heckman, T. M., et al. 2001, ApJ, 550, 724
Leitherer, C., Ortiz, O., Paula, A., Bresolin, F., et al. 2010, ApJ, 189, 309
Liu, X., Shapley, A. E., Coil, A. L., Brinchmann, J., & Ma, C.-P. 2008, ApJ, 678, 758
McGaugh, S. S. 1991, ApJ, 380, 140
Mannucci, F., Cresci, G., Maiolino, R., et al. 2009, MNRAS, 398, 1915
Mannucci, F., Cresci, G., Maiolino, R., Marconi, A., & Gnerucci, A. 2010, MNRAS, 408, 2115
Mannucci, F., Salvaterra, R., & Campisi, M. A. 2011, MNRAS, 414, 1263
Maier, C., Meisenheimer, K., & Hippelein, H. 2004, A&A, 418, 475
Maiolino, R., Nagao, T., Grazian, A., et al. 2008, A&A, 488, 463
Mehlert, D., Tapken, C., Appenzeller, I., et al. 2006, A&A, 455, 835
Mouhcine, M., Gibson, B. K., Renda, A., & Kawata, D. 2008, A&A, 486, 711
Murray, N., Quataert, E., & Thompson, T. A. 2005, ApJ, 618, 569
Nagamine, K., Fukugita, M., Cen, R., & Ostriker, J. P. 2001, MNRAS, 558, 479
Nagao, T., Maiolino, R., & Marconi, A. 2006, A&A, 459, 85
Nakajima, K., Ouchi, M., Shimasaku, K., et al. 2012, ApJ, 745, 12
Oppenheimer, B. D., & Davé, R. 2008, MNRAS, 387, 577
Pagel, B. E. J., Edmunds, M. G., Blackwell, D. E., et al. 1979, MNRAS, 189, 95
Panter, B., Jimenez, R., Heavens, A. F., & Charlot, S. 2008, MNRAS, 391, 111
Pettini, M., & Pagel, B., E.J. 2004, MNRAS, 348, L49
Pettini, M., Ellison, S. L., Steidel, C. C., & Bowen, D. V. 1999, ApJ, 510, 576
Pettini, M., Steidel, C. C., Adelberger, K. L., Dickinson, M., & Giavalisco, M. 2000, ApJ, 528, 96
Pettini, M., Shapley, A. E., Steidel, C. C., Cuby, J.-G., et al. 2001, ApJ, 554, 981
Pozzetti, L., Bolzonella, M., Lamareille, F., et al. 2007, A&A, 474, 443
Quider, A. M., Pettini, M., Shapley, A. E., & Steidel, C. C. 2009, MNRAS, 398, 1263
Quider, A. M., Shapley, A. E., Pettini, M., Steidel, C. C., & Stark, D. P. 2010, MNRAS, 402, 1467
Richard, J., Jones, T., Ellis, R., et al. 2011, MNRAS, 416, 463
Rix, S. A., Pettini, M., Leitherer, C., et al. 2004, ApJ, 615, 98
Sanders, N. E., Soderberg, A. M., Valenti, S., et al. 2011 [arXiv:1110.2363]
Salvaterra, R., Ferrara, A., & Dayal, P. 2011, MNRAS, 414, 847
Sakstein, J., Pipino, A., Devriendt, J. E. G., & Maiolino, R. 2011, MNRAS, 410, 2203
Savaglio, S., Glazebrook, K., Le Borgne, D., et al. 2005, ApJ, 635, 260
Shapley, A. E. 2011, ARA&A, 49, 525
Shapley, A. E., Steidel, C. C., Pettini, M., & Adelberger, K. L. 2003, ApJ, 588, 65
Shapley, A. E., Coil, A. L., Ma, C.-P., & Bundy, K. 2005, ApJ, 635, 1006
Siana, B., Teplitz, H. I., Chary, R.-R., Colbert, J., & Frayer, D. T. 2008, ApJ, 689, 59
Somerville, R. S., Hopkins, P. F., Cox, T. J., Robertson, B. E., & Hernquist, L. 2008, MNRAS, 391, 481
Spitoni, E., Calura, F., Matteucci, F., & Recchi, S. 2010, 514, 73
Stark, D. P., Swinbank, A. M., Ellis, R. S., et al. 2008, Nature, 455, 755
Stasiska, G. 2005, A&A, 434, 507
Tassis, K., Kravtsov, A. V., & Gnedin, N. Y. 2008, ApJ, 672, 888
Teplitz, H. I., McLean, I. S., Becklin, E. E., et al. 2000, ApJ, 533, 65
Tissera, P. B., De Rossi, M. E., & Scannapieco, C. 2005, MNRAS, 364, L38
Tornatore L., Borgani S., Dolag K., & Matteucci F. 2007, MNRAS, 382, 1050
Tremonti, C. A., Heckman, T. M., Kauffmann, G., et al. 2004, ApJ, 613, 898
Veilleux, S., Cecil, G., & Bland-Hawthorn, J. 2005, ARAA, 43, 769
Weiner, B. J., Coil, A. L., Prochaska, J. X., et al. 2008, ApJ, 692, 187
Yates, R. M., Kauffmann, G., & Guo, Q. 2011, MNRAS, submitted [arXiv:1107.3145]
Zahid, H. J., Kewley, L. J., & Bresolin, F. 2011, ApJ, 730, 137